ELSEVIER

Journal of Photochemistry and Photobiology A: Chemistry 106 (1997) 61–66

Journal of PHOTOCHEMISTRY AND PHOTOBIOLOGY A: CHEMISTRY

Dual $^3(d-d)$ emission of $[RhL_2Cl_2](PF_6)$ ($L \equiv 2,2'$-bipyridine and 1,10-phenanthroline) in a crystal in the temperature range 77–536 K

Ashraful Islam, Noriaki Ikeda, Koichi Nozaki, Takeshi Ohno *

Department of Chemistry, Graduate School of Science, Osaka University, Toyonaka, Osaka 560, Japan

Abstract

Emission kinetic spectroscopy of $[Rh(2,2'\text{-bipyridine})_2Cl_2](PF_6)$ and $[Rh(1,10\text{-phenanthroline})_2Cl_2](PF_6)$ was studied in crystalline form up to 536 K. A dramatic shift of the emission peak from 14 600 cm^{-1} to 12 800 cm^{-1} and an increase in the full width at half-maximum of the whole spectrum from 2850 cm^{-1} to 5450 cm^{-1} were observed for $[Rh(2,2'\text{-bipyridine})_2Cl_2](PF_6)$ with increasing temperature from 77 to 536 K. The unusual spectral change with temperature can be interpreted in terms of a two $^3(d-d)$ emitting states model. The Franck–Condon energies for the $^3(d-d)$ emissions are determined to be about 3700 cm^{-1} for the excited state of $^3(d-d)_1$ and 6400 cm^{-1} for the excited state of $^3(d-d)_2$. The non-radiative transition of $^3(d-d)_1$ occurs via the following successive processes: $^3(d-d)_1 \rightarrow {}^3(d-d)_2 \rightarrow$ ground state. The well-displaced potential curve of $_3(d-d)_2$ lowers the activation energy of the non-radiative process above 350 K. © 1997 Elsevier Science S.A.

Keywords: Dual $^3(d-d)$ emission; Emission kinetic spectroscopy; $[RhL_2Cl_2](PF_6)$ ($L \equiv 2,2'$-bipyridine, 1,10-phenanthroline)

1. Introduction

Photoinduced electron transfer reactions within donor–acceptor compounds containing d^6 metal ions (Ru(II), Os(II), Rh(III) and Co(III)) in solution and crystalline form at room temperature have been studied in detail [1–7]. In electron transfer processes, the solvation energy and solvent orientation relative to charged solutes are changed and the energy and distance of coordination bonds between the rhodium (or cobalt) ion and the ligands are reorganized to a large extent. The energetics and dynamics of the reorganization of solvation and coordination play a key role in electron transfer reactions.

Reduced complexes of rhodium(II) and cobalt(II), having an electron on the anti-bonding $d\sigma^*$ orbital, are unstable and undergo ligand exchange reactions [8,9] and intersystem crossing [3,4] respectively. The short lifetimes of the reduced species makes the determination of the reorganization energy for the reduction process difficult. However, the Franck–Condon energy of the emission originating from the excited states of $d\pi^5 d\sigma^*$ configuration can be assumed to be close to the reorganization energy of the rhodium redox reaction. The lowest d–d excited state of a rhodium(III) compound in low-temperature rigid glass exhibits a broad emission [10–15]. Increasing temperature produces a shorter lifetime [16–19] and a larger width of emission [19]. Moreover, dissolving a rhodium(III) compound in fluid polar solvents leads to another decay channel of the excited state resulting in ligand exchange reactions [14–17,19–21]. It is important to determine the characteristics of the lowest excited d–d state as well as the higher excited d–d states of the d^6 metal ion, and the solvation effects, in order to interpret the electron transfer dynamics. For this purpose, excited d–d states of ruthenium(II) and rhodium(III) compounds over a wide temperature range have been examined in crystalline form [22,23]. In this paper, solid samples of *cis*-$[RhL_2Cl_2](PF_6)$ ($L \equiv 2,2'$-bipyridine (bpy) and 1,10-phenanthroline (phen)) in the temperature range 77–586 K were investigated to clarify the role of displaced excited d–d states in both radiative and non-radiative transitions.

2. Experimental details

2.1. Materials

cis-$[Rh(bpy)_2Cl_2](PF_6)$ and *cis*-$[Rh(phen)_2Cl_2](PF_6)$ were prepared by the method of Gidney et al. [24]. The Rh(III) complexes were recrystallized several times and light yellow crystals were grown from acetone–acetonitrile (1 : 4)

* Corresponding author.

PII S1010-6030(97)00040-3

by slow evaporation of the solvent at room temperature. All emission measurements were carried out on the crystalline form.

2.2. Measurements

For the emission measurements, the THG (355 nm; full width at half-maximum (FWHM), 10 ns) pulse of a *Q*-switched Nd^{3+}:YAG laser (Quantel YG580) was used to excite the sample. The emitted light, monitored at 60° from the excitation beam, passed through a grating monochromator (Jasco CT250) with a silicon diode array (Hamamatsu S3901-512Q). The detector sensitivity was corrected using a bromine lamp (Ushio IPD 100 V500 WCS). For decay time measurements, the excitation laser intensity was attenuated to less than approximately 100 μJ per pulse by neutral density filters to avoid non-linear photoprocesses [23]. A cryostat (Oxford ND-1740) with a temperature controller (Oxford ITC-4) was used in the temperature region 77–300 K. Above 300 K, the sample to be taken in a capillary quartz cell were placed into an aluminium block and heated by a hot plate.

2.3. Emission spectral fitting

For emission spectral fitting, a single-mode Franck–Condon analysis of the emission spectra was used [25]. Eq. (1) was used in the fitting procedure, where $I(\nu)$ is the relative emitted light intensity at a certain energy (in wavenumbers)

$$I(\nu)=\left(\frac{\bar{\nu}}{\bar{\nu}_{0-0}}\right)^3 \sum_{n_L=0} \exp(-S_L)\frac{S_L^{n_L}}{n_L!}\sqrt{\frac{4\ln 2}{\pi\Delta\bar{\nu}_{1/2}^2}} \times\exp\left[-\frac{4\ln 2(\bar{\nu}-\bar{\nu}_{0-0}+n_L\bar{\nu}_L)^2}{\Delta\bar{\nu}_{1/2}^2}\right] \quad (1)$$

In Eq. (1), n_L is the vibrational quantum number for a low-frequency vibrational progression of the accepting mode, S_L is the electron–vibrational coupling constant or Huang–Rhys factor, which is related to the distortion in the molecular coordinate corresponding to the low-frequency accepting mode, ν_{0-0} is the energy difference between the excited and ground states in the lowest energy vibrational levels and $\Delta\bar{\nu}_{1/2}$ is the FWHM of the vibronic lines of the emission; it includes contributions from both very low-frequency modes and inhomogeneous broadening depending on the temperature. The value of $\Delta\bar{\nu}_{1/2}$ is assumed to be equal to that of the metal-to-ligand charge transfer (MLCT) phosphorescence (550 cm^{-1}) of a single crystal of $[Ru(bpy)_3](PF_6)_2$ at 77 K [23] and increases with the square root of the temperature. $\bar{\nu}_L$ is taken as a typical metal–ligand stretching frequency of 400 cm^{-1}. The values of S_L and $\bar{\nu}_{0-0}$ were varied to obtain the best fit of the observed spectra.

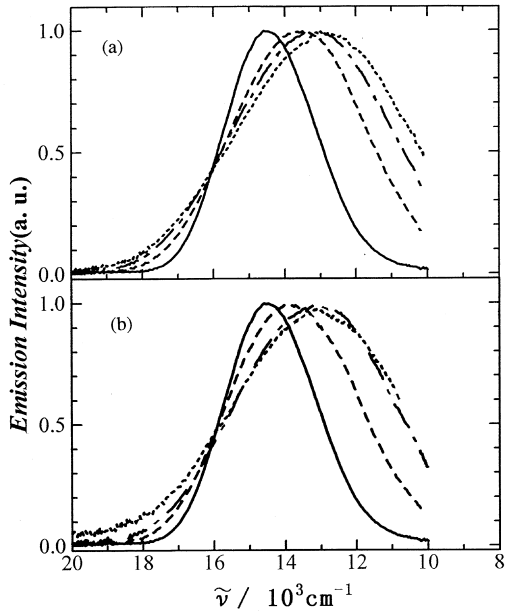

Fig. 1. Temperature dependence of the emission spectra of Rh(III) compounds: (a) $[Rh(bpy)_2Cl_2](PF_6)$: ———, 77 K; - - -, 297 K; – · –, 441 K; · · ·, 536 K; (b) $[Rh(phen)_2Cl_2](PF_6)$: ———, 77 K; - - -, 298 K; – · –, 436 K; · · ·, 528 K. The intensities of the emission peaks are normalized.

3. Results

3.1. Emission spectra

Anhydrous crystals of $[Rh(bpy)_2Cl_2](PF_6)$ and $[Rh(phen)_2Cl_2](PF_6)$ at 77 K emit a broad emission on excitation at the tail of the strong π–π^* absorption band [26]. The broad emission is denoted as EM_1. Fig. 1 shows the temperature-dependent emission spectra of $[Rh(bpy)_2Cl_2](PF_6)$ and $[Rh(phen)_2Cl_2](PF_6)$ crystals in the temperature range 77–536 K. The emission of $[Rh(bpy)_2Cl_2](PF_6)$ crystal displays a dramatic shift in the peak energy from about 14 600 cm^{-1} to 12 800 cm^{-1} and an increase in the FWHM from about 2850 cm^{-1} to 5450 cm^{-1} with increasing temperature from 77 to 536 K as shown in Fig. 1 and Table 1. Similar emission spectra were observed for $[Rh(phen)_2Cl_2](PF_6)$ in the same temperature range, but the emission bandwidths were a little narrower than for $[Rh(bpy)_2Cl_2](PF_6)$.

The spectral profiles of EM_1 were analysed in terms of the Franck–Condon factor of a low-frequency vibrational mode outlined above. The frequency of this mode was fixed as there was insufficient resolution in the spectra until 77 K to determine it accurately. The values of the parameters $\bar{\nu}_L$, S_L and $\bar{\nu}_{0-0}$ were obtained from the spectral fitting procedure of the 77 K emission spectrum of the complex as shown in Fig. 2. It should also be noted that $\bar{\nu}_{0-0}$ cannot be rigorously determined, because of the approximations required in the spectral modelling of the lower frequency modes and the lack of spectral resolution.

The parameters derived from the low-temperature spectrum do not provide a fit for the higher temperature emissions,

Table 1
Peak energy ($\tilde{\nu}_{max}$), full width at half-maximum (FWHM) and lifetime of d–d emission of rhodium(III) crystals at 77, 297 and 536 K

Compound	77 K			297 K			536 K		
	$\tilde{\nu}_{max}$ (cm^{-1})	FWHM (cm^{-1})	τ (10^{-6} s)	$\tilde{\nu}_{max}$ (cm^{-1})	FWHM (cm^{-1})	τ (10^{-6} s)	$\tilde{\nu}_{max}$ (cm^{-1})	FWHM (cm^{-1})	τ (10^{-6} s)
$[Rh(bpy)_2Cl_2](PF_6)$	14600	2850	98	13500	4250	24	12800	5450	0.2
$[Rh(phen)_2Cl_2](PF_6)$	14600	2700	71	13800 [a]	4200 [a]	21 [a]	13000 [b]	5400 [b]	0.1 [b]
$[Rh(bpy)_2Cl_2]^+$	14200 [c]	3500 [c]	46 [c]	–	–	–			
$[Rh(phen)_2Cl_2]^+$	14100 [d]	–	41 [d]	14300 [e]	–	0.7 [e]			

[a] Data at 298 K.
[b] Data at 528 K.
[c] In ethanol–methanol (from Ref. [19]).
[d] In ethanol–methanol (from Ref. [11]).
[e] At room temperature in acetonitrile (from Ref. [18]).

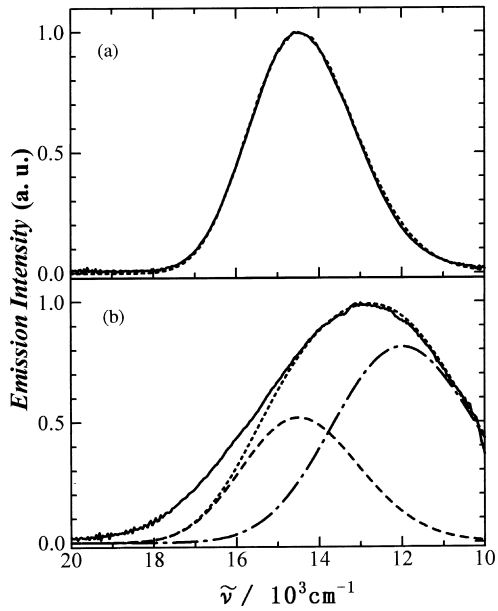

Fig. 2. Emission spectrum (———) and calculated best fit (· · ·) using Eq. (1) and the spectral fitting parameters in Table 2 at 77 K (top) and 536 K (bottom) for $[Rh(bpy)_2Cl_2](PF_6)$ crystal; - - -, calculated spectrum of EM_1; – · –, calculated spectrum of EM_2.

which exhibit large red shifts and much larger FWHM. The presence of two emitting states is postulated for these complexes. Another emission with a lower energy peak, denoted by EM_2, is presumed to originate from the second lowest excited state with a larger $\bar{\nu}_{0-0}$ value (500 cm^{-1} larger than the largest $\bar{\nu}_{0-0}$ value of EM_1). The broader emission spectra at higher temperatures are decomposed into two emissions, EM_1 and EM_2, in the following ways. The temperature-independent values of S_L and $\bar{\nu}_{0-0}$ for EM_1 were taken as those determined at 77 K. The temperature-independent S_L and ν_{0-0} values for EM_2 and the temperature-dependent intensity ratio of EM_2 to EM_1 were varied to obtain a fit of the higher temperature spectra. The emission spectra of $[Rh(bpy)_2Cl_2](PF_6)$ at 536 K are shown to be decomposed into two spectra in Fig. 2. The values of the spectral fitting parameters. i.e. $\bar{\nu}_{0-0}$, S_L and ν_L, are collected in Table 2. The EM_2 peak is so far from the EM_1 peak that both S_L and $\bar{\nu}_{0-0}$ for EM_2 were determined nearly independently of the intensity ratio of EM_2 to EM_1. The emission spectra at 536 K do not provide an accurate fit in the higher energy region due to hot bands occurring in this energy region.

3.2. Emission decay

The emissions of $[Rh(bpy)_2Cl_2](PF_6)$ and $[Rh(phen)_2Cl_2](PF_6)$ decay via a single exponential mode over the whole temperature range studied. The temperature dependences of the emission decays are shown in Fig. 3. The decay rate of the emission gradually increases up to 150 K with increasing temperature. Above 350 K, the non-radiative decay rate increases abruptly as the temperature increases. The temperature-dependent decay rates were fitted using an Arrhenius-type equation (Eq. (2)) with three decay processes

$$k_{obs}(T) = A_L \exp(-E_L/RT) + A_M \exp(-E_M/RT) + A_H \exp(-E_H/RT) \quad (2)$$

where A_L, E_L, A_M, E_M and A_H, E_H are the frequency factor and activation energy for the low-, medium- and high-tem-

Table 2
Emitting state (ES), 0–0 energy ($\tilde{\nu}_{0-0}$), Huang–Rhys factor (S_L) and Franck–Condon energy (FC) of emissions

Compound	ES (cm^{-1})	$\tilde{\nu}_{0-0}$ (cm^{-1})	S_L	FC (cm^{-1})
$[Rh(bpy)_2Cl_2](PF_6)$	$^3(d-d)_1$	18 300	11	3700
	$^3(d-d)_2$	18 400	18	6400
$[Rh(phen)_2Cl_2](PF_6)$	$^3(d-d)_1$	18 000	10	3400
	$^3(d-d)_2$	18 200	17	5900

perature regions respectively. Values of A_L and E_L were determined first and then the other parameters were obtained by subtracting the decay rate of the lower temperature decay channel(s). The parameters obtained are summarized in Table 3.

4. Discussion

4.1. Closely lying d–d excited states

The *cis*-[Rh(bpy)$_2$Cl$_2$](PF$_6$) and *cis*-[Rh(phen)$_2$Cl$_2$](PF$_6$) complexes at 77 K exhibit a broad emission (EM_1) similar to the emission of [Rh(bpy)$_2$Cl$_2$]Cl powder [10], which has been attributed to the $^3(d-d)$ excited state with a configuration $d\pi^5 d\sigma^*$. The emission spectrum of [Rh(NH$_3$)$_6$][Rh(CN)$_6$] recorded at 78 K reveals a structural feature, and cooling from 78 to 4.2 K causes only an increased clarity of the fine structure of the vibronic bands [12]. At 77 K, both [Rh(bpy)$_2$Cl$_2$](PF$_6$) and [Rh(phen)$_2$Cl$_2$](PF$_6$) crystals show an emission peak maximum at 14 600 cm^{-1}, which is red shifted to about 400 cm^{-1} in rigid glass. The broad band of EM_1 of [Rh(bpy)$_2$Cl$_2$](PF$_6$) and [Rh(phen)$_2$Cl$_2$](PF$_6$) is composed of a progression of vibronic lines, which are not seen because of the larger FWHM than the vibrational frequency of the accepting mode (Fig. 2). Satisfactory fits were obtained with $\bar{\nu}_L = 400$ cm^{-1} and $S_L \approx 11$ for the compounds. The magnitude of S_L is similar to that of the low-temperature emission of Rh(III) compounds [12,14].

On increasing the temperature of [Rh(bpy)$_2$Cl$_2$](PF$_6$) up to 536 K, the peak shift of the emission is 1800 cm^{-1} with a considerable reduction in intensity and the FWHM of the whole band increases in width from 2850 cm^{-1} to 5450 cm^{-1}. Good fits for the higher temperature spectra could not be obtained using the parameters of EM_1. The temperature-dependent emission spectral change can be interpreted in terms of the two emitting states model described above. The $^3(d-d)_2$ state responsible for EM_2 lies about 150 cm^{-1} above the $^3(d-d)_1$ state and is more displaced from the ground state than $^3(d-d)_1$ (Table 2). The Franck–Condon energies of EM_1 and EM_2 are determined to be 3700 cm^{-1} and 6400 cm^{-1} respectively from the $\bar{\nu}_{0-0}$ and emission peak. Likewise, the Franck–Condon energies of EM_1 and EM_2 for [Rh(phen)$_2$Cl$_2$](PF$_6$) are determined to be 3400 cm^{-1} and 5900 cm^{-1} respectively. The intense EM_2 peak, as shown in Fig. 2, suggests that EM_2 can be attributed to a symmetry-allowed transition from $^3B_1$ and $^3B_2$ of the C_{2v} group, which originates from $^3T_{1g}$ of the O_h group in the symmetry reduction. The EM_1 peak can be assigned to a symmetry-forbidden transition from $^3A_2$.

Such a large Franck–Condon energy of the d–d emission (7500 cm^{-1}) was estimated for Rh(bpy)$_2$(*N*-methyl-2-(2-pyridyl)benzimidazole)$^{3+}$ in butyronitrile from the difference in energy between the 0–0 peak of the well-resolved π–π^* emission and the broad d–d emission peak at 300 K [27].

A decreasing peak energy and increasing width of the d–d emission with temperature were observed for Rh(3,3′-dimethyl-2,2′-bipyridine)$_3^{3+}$ in rigid solvents [19]. The presence of a slightly higher lying and more displaced d–d excited state may be responsible for the strange temperature dependence of the emission spectrum.

4.2. Three decay channels of ^{3}(d−d) excited states

Both [Rh(bpy)$_2$Cl$_2$](PF$_6$) and [Rh(phen)$_2$Cl$_2$](PF$_6$) crystals show a long emission lifetime at 77 K compared with that in solution (Table 1). At room temperature, [Rh(phen)$_2$Cl$_2$](PF$_6$) exhibits an emission lifetime of 21 μs, which decreases to 0.7 μs in acetonitrile and depends on the type of solvent [18]. The $^3(d-d)$ excited states of both complexes decay via three decay channels as shown in Fig. 3. The weak temperature dependence below 150 K is due to the non-radiative transition via weak coupling (Table 3), because the small value of the frequency factor (10^4 s^{-1}) is characteristic of weak coupling. The temperature-independent non-radiative transition of $^3(d-d)$ has been observed to decrease on deuteration of NH$_3$ for Rh(NH$_3$)$_6^{3+}$ [20,21].

The decay channel above 150 K requires thermal excitation to an intermediate state. The activation energy of internal conversion can be calculated from the differences in the bottom energy, curvature and displacement of the potential curve to a first approximation. Since the small value of E_M implies that the energy level of the intermediate is very close to that of $^3(d-d)_1$, $^3(d-d)_2$ is the most probable candidate for the intermediate. Provided that the potential curves of the excited

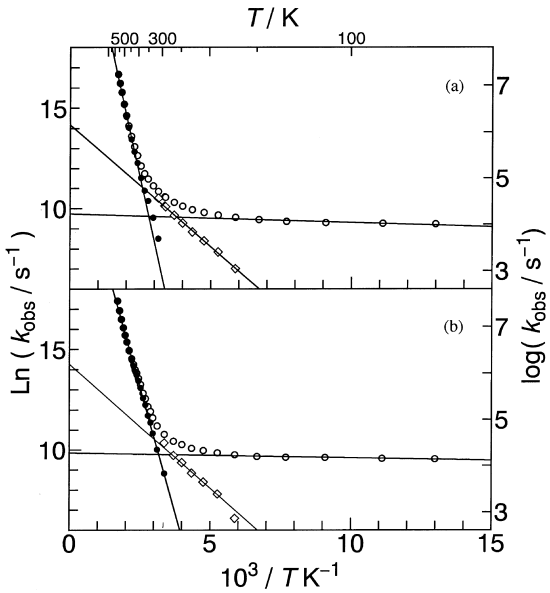

Fig. 3. Calculated fits of the temperature dependence of the emission decay rate constant (k_{obs}) of [Rh(bpy)$_2$Cl$_2$](PF$_6$) (a) and [Rh(phen)$_2$Cl$_2$](PF$_6$) (b). The raw data are plotted as open circles (○). The open squares (□) denote the medium-temperature region data (150–350 K) after subtracting the contribution of the low-temperature decay channel (less than 150 K), and the filled circles (●) denote the high-temperature region data (greater than 350 K) after subtracting the contribution of the low- and medium-temperature decay channels.

Table 3
Frequency factor (A) and activation energy (E) of the temperature-dependent decay of the luminescence for the low- (L), medium- (M) and high-temperature (H) channels

Compound	A_L (10^4 s^{-1})	E_L (cm^{-1})	A_M (10^6 s^{-1})	E_M (cm^{-1})	A_H (10^{11} s^{-1})	E_H (cm^{-1})
$[Rh(bpy)_2Cl_2](PF_6)$	1.7	30	1.5	850	7.0	4400
$[Rh(phen)_2Cl_2](PF_6)$	1.9	18	1.6	860	1.5	3400

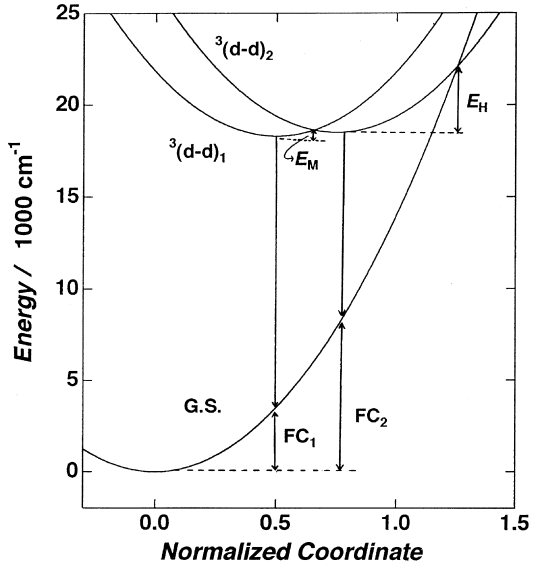

Fig. 4. Schematic potential energy diagram for $[Rh(bpy)_2Cl_2](PF_6)$ and $[Rh(phen)_2Cl_2](PF_6)$. $^3(d-d)_1$ and $^3(d-d)_2$ are the lowest and second lowest excited $^3(d-d)$ states respectively.

d–d states are similar with respect to curvature, the energy gap between them is estimated to be 150 cm^{-1} from the difference in their Franck–Condon energies and the magnitude of E_M. The large radiative rate of $^3(d-d)_2$ is responsible for the large frequency factor (10^6 s^{-1}) of the medium-temperature decay channel compared with $^3(d-d)_1$.

Above 350 K, the non-radiative decay rate increases abruptly with increasing temperature. Another decay channel is opened by thermal agitation of $[Rh(bpy)_2Cl_2](PF_6)$ and $[Rh(phen)_2Cl_2](PF_6)$ with frequency factors of 7.0×10^{11} s^{-1} and 1.5×10^{11} s^{-1} and activation energies of 4400 cm^{-1} and 3400 cm^{-1} respectively. The potential energy diagram of $[Rh(bpy)_2Cl_2](PF_6)$ crystals is shown in Fig. 4, where FC_1 and FC_2 are the Franck–Condon energies of the emission for the lowest excited $^3(d-d)_1$ state and the second lowest excited $^3(d-d)_2$ state respectively. The non-radiative transition of the lowest excited state occurs via a potential crossing between the $^3(d-d)_2$ and ground state (GS). From the spectral fitting data of $[Rh(bpy)_2Cl_2](PF_6)$, the values of FC_1 and FC_2 are calculated to be 3700 cm^{-1} and 6400 cm^{-1} respectively. The activation energy of E_H to pass the crossing seam between the potential curves of $^3(d-d)_2$ and GS can be expressed in terms of the 0–0 emission energy of $^3(d-d)_2$ and the reorganization energy (λ) as $E_H = (\bar{\nu}_{0-0}-\lambda)^2/4\lambda$. The reorganization energies of the non-radiative decay of $[Rh(bpy)_2Cl_2](PF_6)$ and $[Rh(phen)_2Cl_2](PF_6)$ are estimated to be 7200 cm^{-1} and 7800 cm^{-1} respectively from E_H, i.e. slightly larger than the Franck–Condon energy of EM_2.

The high exoergonicity of intersystem crossing (18 200 cm^{-1}) suggests that the conversion process occurs via the potential crossing seams with the vibrationally excited ground state in addition to classical potential crossing. Such coupling of the non-radiative electronic transition to vibrational modes has been verified for exoergonic electron transfer reactions [28–30]. Since the potential crossing to the vibrationally excited ground state requires less thermal excitation compared with classical potential crossing, the exoergonic intersystem crossing accompanied by n quanta of vibration reduces the extent of activation energy (E_H) and the extrapolated intercept (A_H) as a result. This, as well as the small electronic coupling of intersystem crossing, may be associated with the smaller magnitude of the intercept (A_H) (two orders of magnitude smaller than the vibrational frequency).

The more displaced d–d excited state of *cis*-$[Rh(bpy)_2X_2]^+$ ($X\equiv Cl^-$ and Br^-) may lead to the dissociation of one of the halogen ions at higher temperatures in fluid solution. The high photochemical aquation yields of *cis*-$[Rh(NH_3)_4X_2]^+$ [16] and *cis*-$[Rh(1,3\text{-propanediamine})_2X_2]^+$ [17] in water compared with the trans forms may be ascribed to the more displaced and shallow potential curve of $^3(d-d)_2$.

References

[1] K. Nozaki, T. Ohno, M. Haga, J. Phys. Chem. 96 (1992) 10 880.
[2] M.T. Indelli, C.A. Bignozzi, A. Harriman, J.R. Schoonover, F. Scandola, J. Am. Chem. Soc. 116 (1994) 3768.
[3] X. Song, Y. Lei, S.V. Wallendal, M.W. Perkovic, D.C. Jackman, J.F. Endicott, D.P. Rillema, J. Phys. Chem. 97 (1993) 3225.
[4] A. Yoshimura, K. Nozaki, N. Ikeda, T. Ohno, J. Phys. Chem. 100 (1996) 1637.
[5] L. De Cola, V. Balzani, F. Barigelletti, L. Flamigni, P. Belser, A. von Zelewsky, M. Frank, F. Vögtle, Inorg. Chem. 32 (1993) 5228.
[6] K. Nozaki, N. Ikeda, T. Ohno, New J. Chem. 20 (1996) 739.
[7] T. Iguro, N. Ikeda, T. Ohno, Inorg. Chim. Acta 226 (1994) 203.
[8] M. Kirch, J.-M. Lehn, J.-P. Sauvage, Helv. Chim. Acta 62 (1979) 1345.
[9] S.-F. Chan, M. Chou, C. Creutz, T. Matsubara, N. Sutin, J. Am. Chem. Soc. 103 (1981) 369.
[10] T.R. Thomas, G.A. Crosby, J. Mol. Spectrosc. 38 (1971) 118.
[11] M.K. DeArmond, J. Hillis, J. Chem. Phys. 54 (1971) 2240.
[12] K. Hakamata, A. Urushiyama, H. Kupka, J. Phys. Chem. 85 (1981) 1983.
[13] S.C. Weaver, D.S. McClure, Inorg. Chem. 31 (1992) 2814.

[14] M.E. Frink, S.D. Sprouse, H.A. Goodwin, R.J. Watts, P.C. Ford, Inorg. Chem. 27 (1988) 1283.
[15] L.J. McClure, P.C. Ford, J. Phys. Chem. 96 (1992) 6640.
[16] D.A. Sexton, L.H. Skibsted, D. Magde, P.C. Ford, Inorg. Chem. 23 (1984) 4533.
[17] L.H. Skibsted, M.P. Hancock, D. Magde, D.A. Sexton, Inorg. Chem. 23 (1984) 3735.
[18] T. Ohno, S. Kato, Bull. Chem. Soc. Jpn. 57 (1984) 3391.
[19] M. Nishizawa, T.M. Suzuki, S.D. Sprouse, R.J. Watts, P.C. Ford, Inorg. Chem. 23 (1984) 1837.
[20] J.D. Petersen, P.C. Ford, J. Phys. Chem. 78 (1974) 1144.
[21] M.E. Frink, P.C. Ford, Inorg. Chem. 24 (1985) 1033.
[22] A. Islam, N. Ikeda, K. Nozaki, T. Ohno, Chem. Phys. Lett. 263 (1996) 209.
[23] N. Ikeda, A. Islam, T. Ohno, to be submitted.
[24] P.M. Gidney, R.D. Gillard, B.T. Heaton, J. Chem. Soc., Dalton Trans. (1972) 2621.
[25] E.M. Kober, J.V. Casper, R.S. Lumpkin, T.J. Meyer, J. Phys. Chem. 90 (1986) 3722.
[26] D.H.W. Carsens, G. Crosby, J. Mol. Spectrosc. 34 (1970) 113.
[27] K. Nozaki, T. Ohno, unpublished results.
[28] M.R. Gunner, P.L. Dutton, J. Am. Chem. Soc. 111 (1989) 3400.
[29] N. Liang, J.R. Miller, G.L. Closs, J. Am. Chem. Soc. 112 (1990) 5353.
[30] M. Bixon, J. Jortner, J. Phys. Chem. 95 (1991) 1941.